Available online at www.sciencedirect.com
SCIENCE DIRECT®
Journal of Nuclear Materials 350 (2006) 47–55
journal of nuclear materials
www.elsevier.com/locate/jnucmat

Mechanical property and microstructural change by thermal aging of SCS14A cast duplex stainless steel

Takuyo Yamada [a,*], Satoshi Okano [b], Hisashi Kuwano [b]

[a] *Institute of Nuclear Safety Systems, Inc., 64 Sata, Mihama-cho, Mikata-gun, Fukui, Japan*
[b] *Muroran Institute of Technology, 27-1, Mizumoto-cho, Muroran, Hokkaido, Japan*

Received 7 June 2004; accepted 12 November 2005

Abstract

The aging behavior, especially saturation, of JIS SCS14A cast duplex stainless steels was investigated on the basis of the mechanical properties and microstructural changes during accelerated aging at 350 °C and 400 °C. The aging behavior of the materials mainly proceeds via two stages. During the first stage, the generation and concentration of the iron-rich and chromium-enriched phase in ferrite occurs by phase decomposition. The first stage corresponds to aging times of up to 3000 h at 400 °C. During the first stage, the ferrite hardness achieved is approximately 600 VHN, and the Charpy impact energy is almost saturated. During the second stage, the precipitated chromium-enriched phase aggregates and coarsens, and the G phase precipitation also occurs. The second stage corresponds to the aging times range of 3000–30 000 h at 400 °C. During the second stage, the ferrite hardness achieved is about 800 VHN; however, further hardening exceeding 600 VHN does not influence the Charpy impact energy.

PACS: 81.40.Cd; 81.30.Mh; 81.40.Np; 82.80.Ej

1. Introduction

Cast duplex stainless steel is used in the primary piping of pressurized water nuclear reactors (PWRs) in the intermediate temperature range of 290 °C–320 °C. However, when they are used in this temperature range for extended periods of time, they can suffer a loss of toughness and Charpy impact energy [1–3] . Earlier studies circumstantially investigated the mechanical properties, Charpy impact energy, tensile test results, and hardness for the aging temperature range of 300 °C–400 °C [1–3]. According to these studies, the loss of Charpy impact energy is almost saturated for aging at 400 °C for up to 10 000 h [1–3]. The saturation time for accelerated aging corresponds to 4–13 years at 320 °C as estimated by an Arrhenius-type relationship, if its activation energy is substituted as 100 kJ/mol. This means that the materials are used in the saturated state for 70% of their operating life, if the operating life is taken as 40 years. Since the cast duplex stainless steels degraded while in service, some researchers studied the fatigue [4], corrosion fatigue [5], and stress corrosion cracking [6,7] properties of the aged

* Corresponding author. Tel.: +81 (0) 770 37 9111; fax: +81 (0) 770 37 2009.
E-mail address: yamada@inss.co.jp (T. Yamada).

0022-3115/$ - see front matter © 2005 Elsevier B.V. All rights reserved.
doi:10.1016/j.jnucmat.2005.11.008

materials. Therefore, it is important to evaluate the degradation time and the properties of the aged materials, particularly at the saturated state.

Microstructural studies of these materials reported phase decomposition to be the main reaction, wherein the ferrite decomposes into iron-rich α and chromium-enriched α' [2,8–11]. The following were reported as secondary reactions: G phase precipitation in ferrite [12–15], carbide [12–14], nitride [13], and γ_2 phase [15] precipitation at the grain boundaries. All microstructural changes, more or less, affect the properties of the material, and the microstructural reactions are completed at the thermodynamic equilibrium state at the intermediate temperature. Hence, the saturation time of the aged materials should be defined on the basis of microstructural phenomena.

The aim of this study is to evaluate the aging kinetics of cast duplex stainless steel, particularly the saturation time and the properties of the aged and saturated materials, on the basis of the changes in the microstructure and mechanical properties during aging. The mechanical properties of aged materials were evaluated by Charpy impact energy and Vickers microhardness. The microstructural changes of aged materials, especially phase decomposition and G phase precipitation, were measured by three-dimensional atom probe (3-DAP) analysis, Mössbauer measurement, and transmission electron microscope (TEM) observation. Additionally, the effects of the microstructural products on the mechanical properties of aged materials are also estimated.

2. Experimental procedure

2.1. Specimens

The chemical compositions of the cast duplex stainless steel SCS14A (equivalent to CF8M) centrifugal castings containing 8%, 15%, and 23% ferrite phase, denoted by F8, F15, and F23, respectively, are shown in Table 1. The chemical compositions of each phase are shown in Table 2. Chromium and molybdenum are enriched in the ferrite phase, and nickel is enriched in the austenite phase. The bulk chemical compositions of the three materials differ, but the chromium and nickel concentrations of the ferrite and austenite are almost the same.

The as-received heat treatment involves holding the SCS14A steels for 7.5 h at 1100 °C for homogenization, followed by water quenching. Then, they were aged at temperatures of 350 °C and 400 °C for up to 30 000 h using an electric furnace in air. After aging, several aged materials underwent recovery heating (RH) at 550 °C for 1 h to selectively remove the phase decomposition.

Table 1
Chemical compositions of SCS14A[a] (wt%)

	C	Si	Mn	P	S	Ni	Cr	Mo	N
Spec.	0.08	1.50	1.50	0.040	0.040	9–12	18–21	2–3	–
F23	0.044	1.46	0.68	0.029	0.016	9.57	20.02	2.23	0.0501
F15	0.039	1.07	0.84	0.023	0.008	9.28	18.80	2.14	0.0558
F8	0.047	0.79	0.90	0.026	0.017	10.67	18.85	2.22	0.0562

[a] Mill sheet data.

Table 2
Chemical composition of each phase[a] (wt%)

	Fe	Ni	Cr	Si	Mo	Mn
F23α	63.78	5.57	25.52	1.67	2.91	0.55
F15α	64.67	5.17	24.62	1.35	3.39	0.80
F8α	63.55	5.54	25.32	1.05	3.65	0.89
F23γ	66.28	9.46	20.13	1.40	1.84	0.89
F15γ	66.98	9.15	19.64	1.24	2.02	0.97
F8γ	65.82	10.0	20.03	0.94	2.20	1.01

[a] Analyzed by EDX at 20 kV using standardless method.

2.2. Charpy impact energy and vickers microhardness

Charpy specimens were machined from the unaged and aged SCS14A centrifugal castings. The specimens had a cross section of 10×10 mm and a length of 55 mm. The notches were 2 mm deep with a 45° angle and a root radius of 0.25 mm. The Charpy impact test was performed at room temperature.

The aging behaviors of ferrite and austenite were evaluated by the 25 g Vickers microhardness test. Because of the small size of the ferrite islands, it was necessary to take the microhardness series of 30 measurements at each aging stage, and to perform a selective statistical analysis. Gonzalez et al. [16] reported that to avoid the influence of the softer underlying austenite on thin ferrite islands, the 100 data of microhardness were measured and arranged in ascending order. From these only the highest 20% hardness values were used. In this study, the highest 10 of 30 measured values were used for simplicity. Vickers microhardness for the austenite phase was obtained as the mean of five measurements, because the error was small.

2.3. Microstructural characterization

The phase decomposition with aging can be evaluated by 3-DAP analysis and Mössbauer spectroscopy. The Cr- or Fe-enriched phase distributions of each aging stage were evaluated by 3-DAP analysis. The mean Cr concentration of the Fe-enriched regions in ferrite during aging was evaluated by the decomposition fraction (y), which was obtained by Mössbauer spectroscopy. G phase precipitation and other precipitations were confirmed by TEM observation and selected area electron diffraction pattern (SADP).

All the specimens for microstructural examination were taken from the inner portion of the pipes. 3-DAP specimens were machined from the materials and electro-polished to obtain needle-like specimens. Mössbauer specimens were mechanically polished and electro-polished to obtain 30–50 μm thin foils. Mössbauer measurement was performed at room temperature. TEM disks were electro-polished in a solution of 450 ml methanol and 50 ml perchloric acid in the temperature range from −50 °C to −60 °C, 40 V. TEM examination was performed at an acceleration voltage of 300 kV with a Hitachi HF3000 transmission electron microscope.

3. Results and discussion

3.1. Change in the Charpy impact energy and microhardness

Fig. 1 shows the change in the Charpy impact energy due to aging at 400 °C and 350 °C. The Charpy impact energies of F23 and F15 decrease rapidly for an aging time shorter than 3000 h. The decrease in impact energy almost saturates after 10 000 h of aging at least in the F23 specimen. As for the F15 specimen, the loss of impact energy does not saturate even after aging at 400 °C for 10 000 h, but tends to saturate after longer periods of aging. As for the F8 specimen, the impact energy does not change even after aging at 400 °C for 10 000 h. The decrease in impact energy during aging is in the order of F23 > F15 > F8. The saturated Charpy impact energy of the three specimen is different depending on the ferrite content.

Fig. 2 shows the Vickers microhardness of ferrite and austenite during aging. The austenite hardness does not change with aging time. But the ferrite hardness markedly increases with aging time. For aging at 400 °C, the ferrite hardness of F23 achieved was about 600 VHN for 3000 h, and the Charpy impact energy was almost saturated. After aging for 3000 h, the ferrite hardness slowly increases to 800 VHN. The rapid ferrite hardening in the

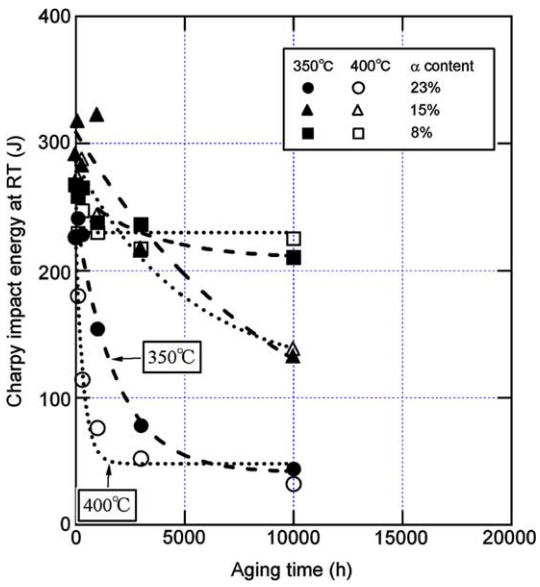

Fig. 1. Charpy impact energy change of SCS14A aged at 400 °C and 350 °C as a function of aging time.

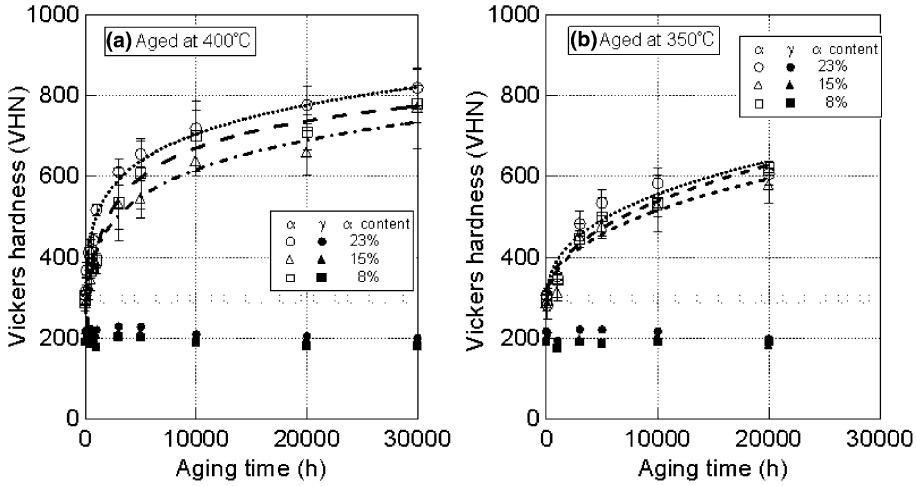

Fig. 2. Vickers hardness change of SCS14A aged at (a) 400 °C and (b) 350 °C as a function of aging time.

300 VHN–600 VHN range is referred to as the first stage, and slow ferrite hardening in the 600 VHN–800 VHN range is referred to as the second stage. The hardening rate at 400 °C is in the order of F23 > F8 > F15. The hardening rate of the three specimens is slightly different. With regard to the aging at 350 °C, the hardening rate is substantially comparable for the three specimens. The hardening trends with aging time are almost similar regardless of the ferrite content.

3.2. Phase decomposition of ferrite

Fig. 3 shows the chromium concentration profiles measured in the ferrite phase of F23 by 3-DAP. The gray surfaces are constructed by connecting positions where the Cr content is 35 at.%. The interior of the gray surface is the region in which the chromium content is enriched more than 35 at.%. In the case of unaged materials, it is natural that the chromium-enriched regions are very few because the mean Cr concentration of the ferrite is 27 at.% (25.5 wt%). After aging at 400 °C for 500 h, the chromium-enriched regions increase much more to produce small islands that are distributed within distances of 3 and 5 nm. After the aging for 10 000 h, most of the Cr-enriched regions are aggregated to construct separated long islands. The ferrite matrix is separated into two regions in which the chromium content is definitely different. The above results indicate that the generation of iron-rich α and chromium-enriched α′ phase in ferrite occurs by phase decomposition after aging at

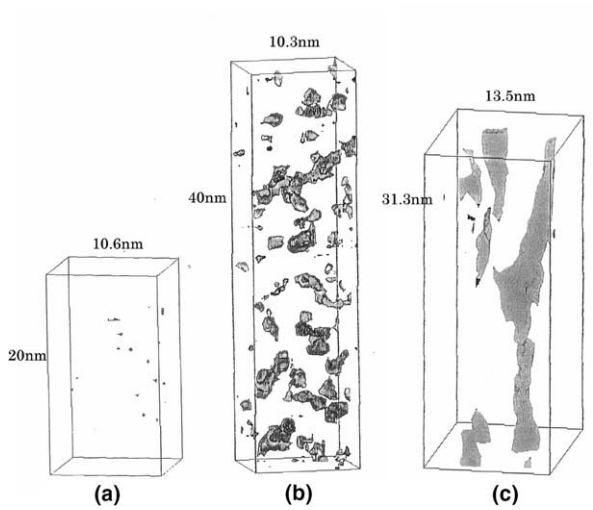

Fig. 3. Isosurface reconstruction of the microstructure in the ferrite phase of F23 materials aged at 400 °C for labeled times (the gray surface encloses the Cr-enriched regions (Cr higher than 35 at.%)): (a) Unaged, (b) 500 and (c) 10 000 h.

400 °C for 500 h. Additionally, the precipitated chromium-enriched α′ phase aggregation and coarsening occur after aging at 400 °C for 10 000 h.

The mean Cr concentration of the Fe-enriched regions in the ferrite during aging was evaluated by the decomposition fraction (y), which was obtained by Mössbauer spectroscopy. The decomposition fraction (y) is given by

$$y = \left(\frac{C_t - C_0}{C_\infty - C_0}\right) \times 100, \quad (1)$$

where C_0 is the mean Cr concentration of the unaged material, C_t is the mean Cr concentration of the Fe-enriched regions of the material aged for t hours, and C_∞ is the mean Cr concentration of the Fe-enriched regions of the final aging condition. The C_∞ value was estimated by the calculated Fe–Cr–Ni ternary phase diagram [10]. The Cr concentration of the Fe-rich regions (C_0,C_t) can be estimated by Eq. (2) [17].

$$\langle H\rangle = 33.5 - 0.36X_{\mathrm{Cr}}, \tag{2}$$

where $\langle H\rangle$ is the mean internal magnetic field of ^{57}Fe in ferrite, and X_{Cr} is the Cr concentration of Fe–XCr–5%Ni ($0 < X_{\mathrm{Cr}} < 60$) system model alloys. The mean internal magnetic field ($\langle H\rangle$) was estimated by calculation from the Mössbauer spectrum according to the method suggested by Le Caer and Dubois [18].

Time variations in the Cr concentration of the ferrite matrix accompanied by phase decomposition are examined on the basis of Eq. (1) by Mössbauer spectroscopy. The change in the mean internal magnetic field ($\langle H\rangle$) is plotted on the left axis of Fig. 4. The values $\langle He\rangle$ are the mean internal magnetic field of the Fe-enriched regions of the final aging condition. The values are obtained from the reference [17], and are depicted by a dotted straight line in the figure.

The value $\langle H\rangle$ increases rapidly during aging at 400 °C for 3000 h, and at 350 °C for 10000 h. The decomposition fraction already achieved 70% and 90% ageing at 400 °C for 3000 h and for at 350 °C for 10000 h, respectively. This indicates that the mean Cr concentration of the ferrite matrix almost reached the final aging condition at the same time. This is in good agreement with the 3-DAP data that observed aggregation and coarsening of Cr-rich regions after aging at 400 °C for 10000 h. The y trends for aging at 400 °C in the F23 and F15 specimens are almost similar, whereas the y trend of F8 indicates a more rapid phase decomposition reaction. In the case of aging at 400 °C, these y trends are in the order F8 > F15, F23. With regard to the aging at 350 °C, y is substantially comparable for the three specimens. The y trends for aging are almost the same regardless of the ferrite content. The early stage of the decomposition fraction in the 0–70 or 90% range is equivalent to the first stage of ferrite hardening. The above results indicate that the concentration of the iron-rich α and chromium-enriched α′ phase in ferrite occurs due to phase decomposition during ageing at 400 °C for 3000 h. But the order of y after 70% is significantly different when compared to the order of the second stage of ferrite hardening. This suggests that some secondary effects influence ferrite hardening in the second stage.

3.3. G phase precipitation

As shown in the TEM image of Fig. 5(a), there are fine precipitates, 4 nm in diameter, in the F23 ferrite aged at 400 °C for 10000 h. The selected area electron diffraction pattern (SADP) consists of two sets of diffraction patterns, that is, strong reflections and weak ones. The former is ascribed to the bcc ferrite. The latter has cube-on-cube orientation to the bcc pattern. The pattern is indexed by an fcc

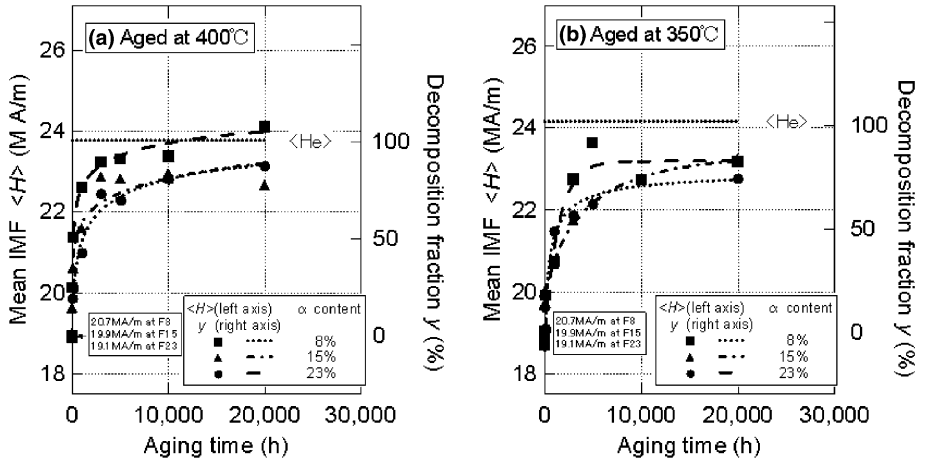

Fig. 4. Mean internal magnetic field $\langle H\rangle$ change of SCS14A aged at (a) 400 °C (b) 350 °C as a function of aging time.

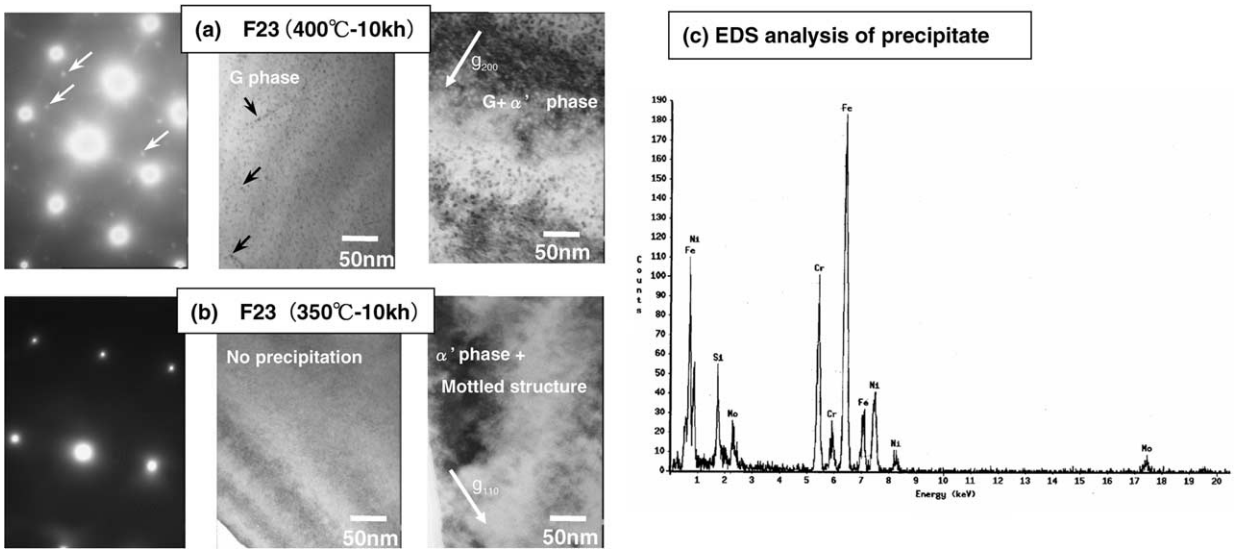

Fig. 5. TEM images and electron diffraction patterns of aged SCS14A for labeled conditions (c) EDS analysis of precipitation.

phase whose lattice parameter is about 1.1 nm. Additionally, the results of the EDS analysis of the precipitates including the surrounding ferrite matrix indicated the presence of 53.7 mass % Fe, 13.3 mass % Ni, 20.2 mass % Cr, 5.9 mass % Mo, 4.9 mass % Si. The compositions of Ni, Si, and Mo are higher when compared to those of the F23 ferrite matrix listed in Table 2. The lattice parameter is nearly equivalent to that of the G phase. Therefore, the precipitates are identified as the G phase. The G phase is clearly observed by TEM during the aging time of 5000 h. In addition to this phase, the precipitation of the Cr-enriched α' phase was confirmed in the ferrite grains though the phase is invisible in Fig. 5(a) due to the unsuitable diffraction conditions between the electron beam and the ferrite crystal orientation. In the case of the aging at 350 °C for 10 000 h, the Cr-enriched α' phase and mottled structures are visible, and SADP is characterized by only a bcc phase as shown in Fig. 5(b). Hence, no G phase precipitation has been observed after 10 000 h.

3.4. Contribution of phase decomposition and G phase to ferrite hardness

Chung et al. [13] and Vitek et al. [14] reported that reheat treatment for 1 h at 550 °C removes the compositional change of ferrite derived by the phase decomposition. To confirm the reheating effect, the F23 specimen aged at 400 °C for 10 000 h was reheated at 550 °C. Mössbauer measurement showed that the mean internal magnetic field was almost identical to that of the unaged material after reheating. However, as shown in Fig. 6, there is no change in the G phase precipitates before and after the reheating. Therefore, reheating is able to remove only the effects of phase decomposition. The hardness of reheated ferrite is presented in Fig. 7. In the case of aging at 400 °C, reheating lowers the ferrite hardness of the aged specimen to intermediate levels, between the aged and the unaged ferrite hardness, for the aging times longer than 5000 h where the G phase exists. Therefore, the ferrite hardness retained after reheating is associated with the G phase. In the case of the specimen aged at 350 °C where no G phase exists, the hardness recovers to the same level as that obtained for unaged reheated ferrite. Thus, the recovery process of the ferrite hardness suggests that ferrite hardening after ageing at 400 °C for 5000 h is interpreted in terms of the mixed contributions from the G phase precipitates the phase decomposition. These reheated ferrite hardness trends of the F15 and F8 specimens for aging at 400 °C are almost similar, whereas the hardening of the F23 specimen occurs more rapidly for the G phase precipitation. In the case of aging at 400 °C, these reheated hardness trends are in the order of F23 > F15, F8. As for the 350 °C aging, the reheated hardness is substantially comparable for the three specimens. The ferrite hardening caused by the G phase is equivalent

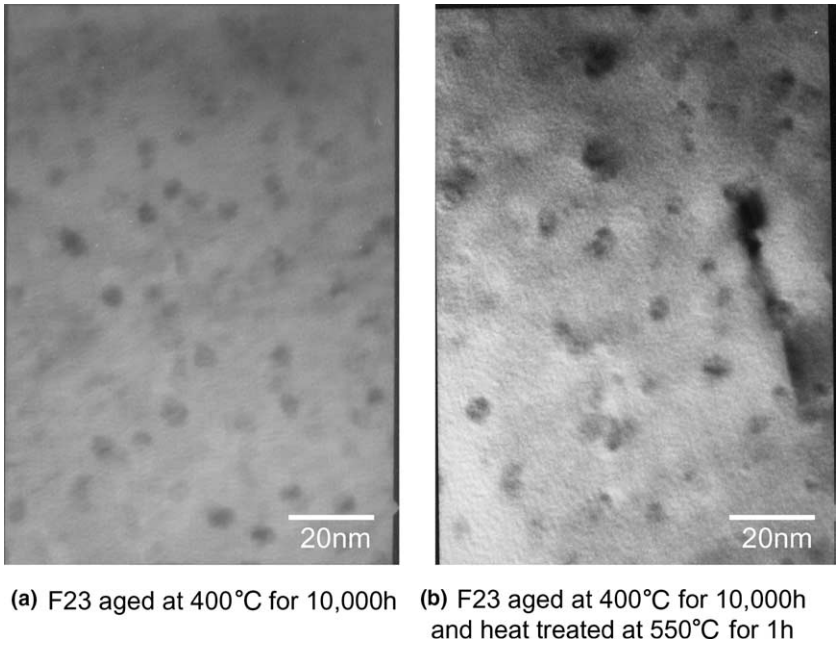

Fig. 6. TEM images of the 23% ferrite aged at 400 °C for 10000 h, (a) before and (b) after heat treatment at 550 °C for 1 h.

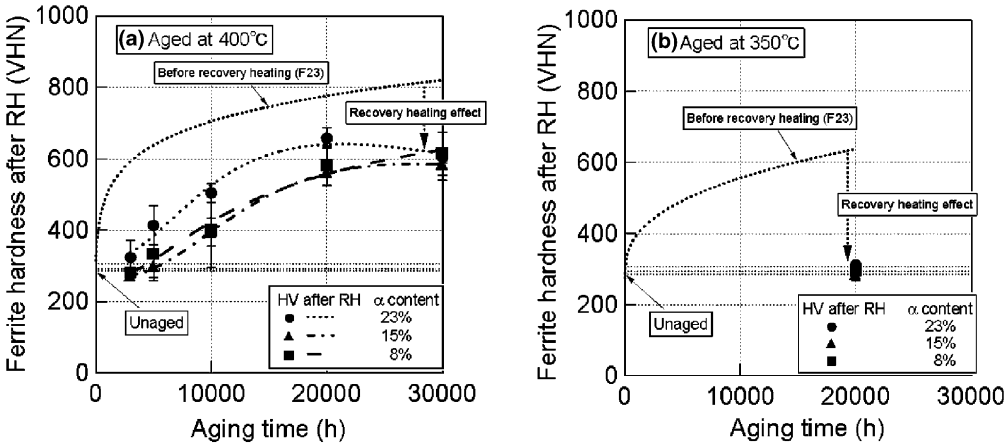

Fig. 7. Vickers hardness changes in SCS14A aged at (a) 400 °C and (b) 350 °C after recovery heating for 1 h at 550 °C as a function of aging time.

to that caused during the second stage of ferrite hardening.

The contribution of the phase decomposition to the ferrite hardness (HV_{PD}) can be estimated by

$$HV_{PD} = HV - \Delta HV_G, \quad (3)$$

where HV is the total ferrite hardness, and ΔHV_G is the incremental hardness due to the G phase. Fig. 8 shows HV_{PD} as a function of the decomposition fraction (y). The HV_{PD} rises with increasing y, and reaches a value of nearly 600 VHN for 70% of y. The HV_{PD} does not exceed 600 VHN even after 70% of y.

As mentioned above, the first stage of rapid ferrite hardening is caused only by phase decomposition. At the second stage of slow ferrite hardening, the precipitated Cr-enriched α' phase aggregation and coarsening occurs, at the same time the G phase precipitation also occurs. Generally, with regard to the precipitation hardening mechanisms, the

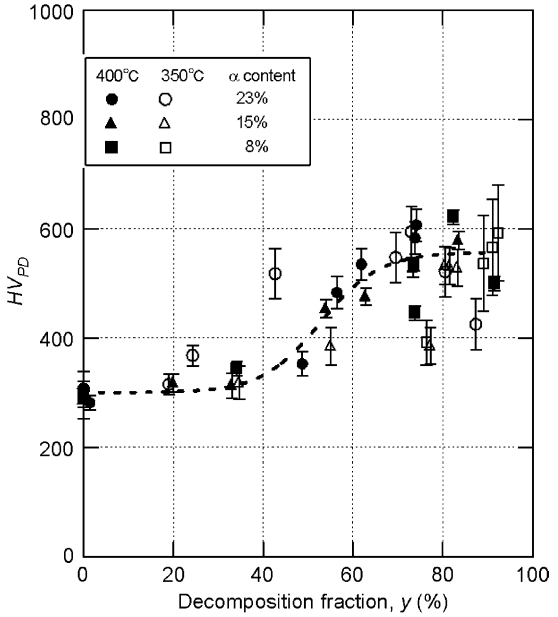

Fig. 8. Increase in ferrite hardness due to phase decomposition (HV_{PD}) plotted against the decomposition fraction (y).

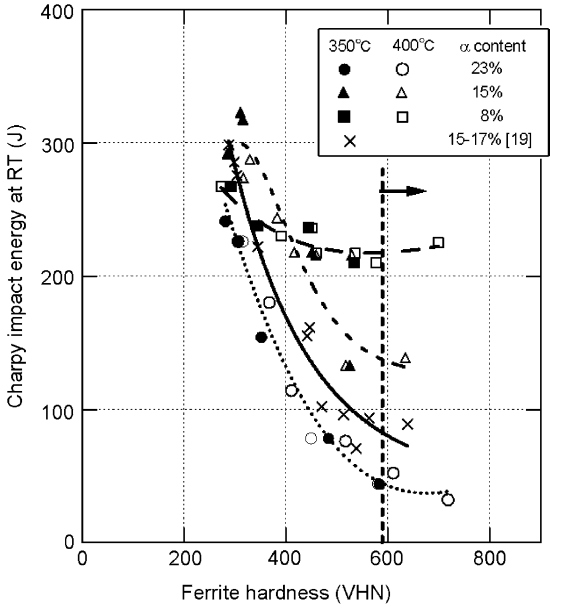

Fig. 9. Relationship between the Charpy impact energy and ferrite hardness.

aggregation and coarsening of precipitation refer to over aging or saturation. Therefore, the second stage of slow ferrite hardening, i.e., exceeding 600 VHN, is mostly caused by G phase precipitation.

3.5. Relationship between the Charpy impact energy and ferrite hardness

As mentioned before, ferrite hardness markedly increases, whereas austenite hardness does not change with aging. This fact suggests a strong correlation between the loss of Charpy impact energy and ferrite hardness. Fig. 9 shows the relationship between the Charpy impact energy and ferrite hardness. In the graph, the Charpy impact energy of 15–17% ferrite containing centrifugal CF8M steel aged at from 300 °C to 450 °C is also plotted [19].

The Charpy impact energy decreases with increasing ferrite hardness up to 600 VHN, and almost saturates where it exceeds 600 VHN. The saturated Charpy impact energy increases linearly with the decrease in the ferrite content as shown in Fig. 10. The extrapolation of the linear relationship to zero percent of ferrite gives a Charpy impact energy of 300 J, which is almost equivalent to the Charpy impact energy of a 316 NG grade austenitic stainless steel. This suggests that the saturated Charpy impact energy can be determined by the ferrite content. As a result, there is a possibility that the ferrite hardness of the final aging condition is approximately 800 VHN or more; however, further hardening exceeding 600 VHN does not influence the Charpy impact energy.

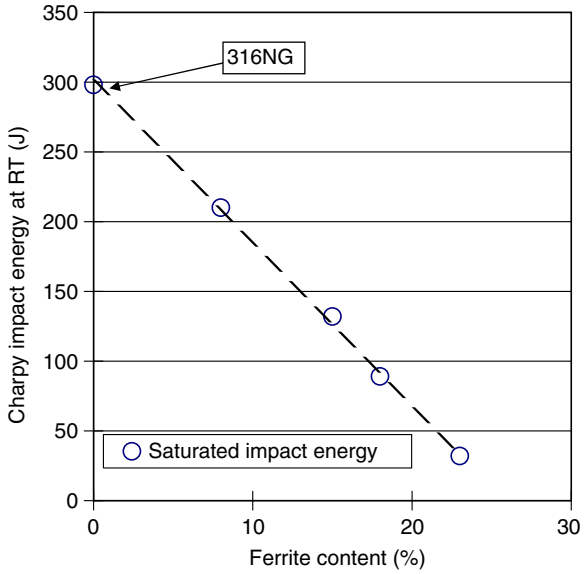

Fig. 10. Relationship between saturated Charpy impact energy and ferrite content.

4. Conclusions

(1) The age hardening process of SCS14A cast duplex stainless steels proceeds through two stages, the first stage is the rapid ferrite hardening during which the ferrite hardness reaches 600 VHN, and then the second stage is the slow ferrite hardening during which the ferrite hardness reaches 800 VHN. The first stage of the rapid ferrite hardening is solely caused due to phase decomposition, which is the generation and concentration of the iron-rich α and chromium-enriched α' phase in ferrite. The second stage of slow ferrite hardening that exceeds 600 VHN, is mostly caused by G phase precipitation.

(2) The Charpy impact energy of the aged materials decreases with ferrite hardening, and then saturates when ferrite hardness exceeds 600 VHN. There is a possibility that the ferrite hardness of the final aging condition is approximately 800 VHN or more; however, further hardening in excess of 600 VHN does not influence the Charpy impact energy. It is suggested that the saturated Charpy impact energy of aged materials is mainly determined by the ferrite content.

Acknowledgements

The authors gratefully acknowledge Dr T. Yoshimura and Dr Y. Ishikawa (Former Hitachi, Ltd.) for the 3-DAP measurements and Dr K. Arioka (INSS, inc.) for valuable comments on the manuscripts.

References

[1] A. Trautwein, W. Gysel, ASTM STP 756 (1982) 165.
[2] O.K. Chopra, SMiRT13 (1995) 349.
[3] G. Bezdikian, ASME (1997) 95.
[4] J.-A.. Le Duff, P. Ould, J.-L. Bernard, Int. J. Pres. Ves. Piping 65 (1996) 241.
[5] L. Iturgoyen, A. Mateo, L. Llanse, M. Anglada, Proc. Int. Cong. Stainless Steels '96 (1996) 355.
[6] T. Yamada, K. Negishi, N. Totsuka, N. Nakajima, Corrosion/2002, Paper No. 02524, 2002.
[7] T. Yamada, K. Negishi, N. Totsuka, N. Nakajima, K. Arioka, Fontevraud 5, Paper 011, 2002.
[8] J.E. Brown, G.D.W. Smith, P.H. Pumphrey, M.K. Miller, in: Fifth International Symposium on Environmental Degradation of Materials in Nuclear Power Systems—Water Reactors, Monterey, August 1991.
[9] P. Auger, F. Danoix, O. Grisot, J.P. Massoud, J.C. Van Duysen, Ann. Phys. Colloq. 20 (1995) C3-143.
[10] T. Miura, H. Kuwano, K. Itoh, Y. Ishikawa, J. Jpn Inst. Metals 63 (1999) 1503.
[11] T. Miura, H. Kuwano, K. Kikuchi, Tetsu-to-hagane 87 (2001) 31.
[12] S.A. David, J.M. Vitec, D.J. Alexander, J. Nondestructive Eval. 15 (1996) 129.
[13] H.M. Chung, T.R. Leax, International Workshop on Intermediate-Temperature Embrittlement Process in Duplex Stainless Steels, 1–2 August, Oxford, England, 1989.
[14] J.M. Vitek, S.A. David, D.J. Alexander, J.R. Keiser, R.K. Nanstad, Acta Metall. Mater. 39 (1991) 503.
[15] Z.W. Hu, S.S. Hsu, X.L. Jiang, Scripta Met. 25 (1991) 645.
[16] J.J. Gonzalez, F. Gutierrez-Solana, L. Sanchez, J. Setien, J. Test Eval. 25 (1997) 154.
[17] K. Itoh, T. Yamaguchi, H. Kuwano, J. Jpn Inst. Mater. 59 (1995) 237.
[18] Le Caer, Dubois, J. Phys. E 12 (1979) 1983.
[19] L. Mraz, F. Matsuda, Y. Kikuchi, N. Naruo, S. Kawaguchi, Trans. JWRI 23 (1994) 213.